

Unraveling Geometric-phase at Conical Intersection by Cavity-enhanced Two-dimensional Electronic Spectroscopy

Yang-Cheng Ye¹, Fulu Zheng^{1,*}, Ajay Jha^{2,3,4,†} and Hong-Guang Duan^{1‡}

¹*Department of Physics, School of Physical Science and Technology, Ningbo University, Ningbo, 315211, P.R. China*

²*Rosalind Franklin Institute, Harwell, Oxfordshire OX11 0QX, United Kingdom*

³*Department of Pharmacology, University of Oxford, Oxford, OX1 3QT United Kingdom*

⁴*Research Complex at Harwell, Rutherford Appleton Laboratory, Didcot OX11 0QX, United Kingdom*

(Dated: November 13, 2025)

The geometric phase is a fundamental quantum mechanical phenomenon uniquely associated with conical intersections (CI) between potential energy surfaces and serves as a definitive signature of their presence. In this study, we propose a novel spectroscopic approach to directly detect the geometric phase using two-dimensional electronic spectroscopy (2DES) enhanced by strong light-matter interactions within an optical cavity. Focusing on a prototypical pentacene dimer undergoing singlet fission, we model the nonadiabatic wave packet dynamics as it evolves through a CI between electronically excited states. The optical cavity enables dynamic modulation of the coupling between the optical field and molecular vibrational modes, allowing precise control over the wave packet pathways. Importantly, we identify a cancellation in the spectral amplitude, arising from phase differences accumulated along different trajectories, which serves as a clear spectroscopic manifestation of the geometric phase (GP). This cavity-enhanced 2DES framework not only enables direct observation of GP effects but also offers a versatile platform for probing ultrafast nonadiabatic processes. Our results provide fundamental insights into topological effects in molecular dynamics and pave the way for experimental strategies in quantum control, photochemistry, and the design of advanced optoelectronic materials.

Conical intersection (CI) is the degenerate point between two potential energy surfaces (PESs), which induced by the degeneration of molecular reaction coordinates [1–3]. This degeneration results in a strong nonadiabatic couplings in the vicinity of the CI, which makes the Born-Oppenheimer approximation breaks down [4]. They act as funnels enabling ultrafast non-radiative transitions between electronic states, typically within tens to hundreds of femtoseconds[5]. CIs play a central role in key molecular processes such as photoisomerization[6], internal conversion[7, 8], and singlet fission[9, 10], which are critical to vision, photosynthesis, and emerging photonic technologies. Understanding their dynamics is essential for accurate modeling of molecular behavior. As such, CIs are a focus of theoretical and computational studies aiming to inform the design of advanced photoactive systems.

Initially deemed theoretical curiosities due to the extreme conditions required for their observation, CI were long considered elusive in real molecules. Advances in ultrafast spectroscopic methods have since provided compelling evidence of their possible existence and significance in diverse polyatomic systems. Mathies and colleagues employed stimulated Raman spectroscopy to track rhodopsin photoisomerization, showing sub-200 fs electronic deactivation [11], while Tahara and colleagues demonstrated ultrafast structural evolution in cis-stilbene, implicating CI-mediated dynamics

[12]. Subsequent transient grating studies by Miller and colleagues revealed even faster isomerisation (< 50 fs) [13], and 2DES experiments further exposed intricate excited-state couplings [14]. Moreover, evidence increasingly links CI to singlet fission processes [9, 10, 15, 16]. Notably, light-induced CIs have recently emerged as a focal topic of study [17–20]. Understanding their mechanistic nature is therefore vital for elucidating nonadiabatic dynamics that govern ultrafast photochemical reactivity and energy relaxation.

Theoretical investigations have shown that nonadiabatic dynamics near CI can be effectively modeled using a simplified two-state-two-mode mode framework[21, 23, 24], where the molecular structural changes are represented by tuning and coupling coordinates[25, 26]. Maxim *et al.* explored these dynamics by simulating time-resolved 2DES, demonstrating that the evolution of wave packets traversing the CI can be discerned through excited-state absorption (ESA) features[27]. Other theoretical studies further support the utility of 2DES as a powerful technique to probe the complex dynamics surrounding CI[28–30]. Extending beyond the optical regime, recent efforts have also proposed exploring these nonadiabatic phenomena using ultrafast X-ray spectroscopy[31–34]. However, it has become evident that rapid electronic deactivation alone does not unambiguously confirm the presence of a CI, as similar ultrafast behavior can arise in systems with avoided crossings (AC)[35]. In light of this, Duan *et al.* compared CI and AC models, revealing that only CI exhibit a geometric phase (GP), a topological feature arising from the wave function’s phase change upon encircling the intersection[36]. This distinction positions the GP as a

* zhengfulu@nbu.edu.cn

† Ajay.Jha@rfi.ac.uk

‡ duanhongguang@nbu.edu.cn

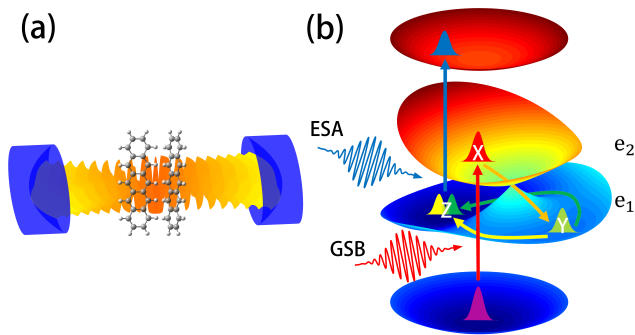


FIG. 1. (a) Schematic representation of a pentacene molecular dimer coupled to an infrared cavity mode. (b) Conceptual energy landscape illustrating vibronic transitions and wave packet evolution.

definitive signature of a CI, providing a crucial criterion for experimentally distinguishing CIs from other nonadiabatic phenomena. Although this phase offers a theoretically rigorous fingerprint for identifying CIs, its experimental detection remains elusive. The subtlety and complexity of observing the GP in real molecular systems highlight a critical gap in current methodologies. Thus, while the GP holds promise as a definitive signature of CIs, realizing its practical detection continues to pose a formidable challenge, underscoring the need for more refined experimental strategies and theoretical tools aimed at isolating and measuring this topological hallmark.

This study presents a theoretical framework for directly detecting the GP associated with CIs via 2DES enhanced by an optical cavity. By modulating the light-matter coupling strength, we isolate spectroscopic features uniquely arising from GP-driven wave packet dynamics. A four-level pentacene dimer model incorporating two vibrational modes and a CI between excited electronic states enables clear observation of these effects on a symmetric potential-energy surface. We identify magnitude cancellation in ESA as a distinct spectroscopic signature of the GP, whose sensitivity to cavity coupling offers a tunable detection mechanism. This work establishes a versatile framework for probing quantum dynamics near CIs and provides a pathway towards controlled exploration of molecular topological phenomena and coherence.

RESULTS AND DISCUSSION

We consider a pentacene dimer for the study of the nonadiabatic dynamics and the associated GP near the CI. It has been demonstrated that the primary singlet fission in pentacene undergoes an ultrafast deactivation of wave packet through the CI [9, 10, 15]. To examine the nonadiabatic dynamics near the CI, we construct a pentacene dimer model, which contains four electronic states, ground S_0 , excited singlet S_1 , the correlated

triplet-pair states ^1TT and ^2TT , respectively. Moreover, two reaction coordinates are considered to strongly couple to the electronic degree of freedoms, which shows a tuning mode with frequency Ω_t and a coupling mode with frequency Ω_c . To consider the cavity-modulated dynamics, we also construct a optical cavity [37, 38], which resonantly oscillate with the coupling mode Ω_c of the molecular dimer. The total Hamiltonian can be written as $H = H_s + H_b + H_{sb}$, H_s represents the Hamiltonian of system, H_b is the environment Hamiltonian and H_{sb} describes the interaction between the system and environment. The detailed Hamiltonian and the parameters are described in the Supporting information (SI).

The results are organized in three parts. First, the intrinsic nuclear wave-packet dynamics of the isolated dimer near the CI are analyzed. Next, the effect of cavity coupling on the nuclear motion and associated interference behavior is examined. Finally, the consequences of these dynamical features are shown in the 2D electronic spectra, where the GP signature becomes optically accessible.

A. Wave-packet dynamics of the dimer

In order to examine the detailed propagation dynamics of the wave packet, we employed the projection procedure of the wave packet onto two reaction coordinates in adiabatic representation [39, 40]. The detailed data treatment of wave-packet dynamics are described in the SI. Fig. 1(a) illustrates the schematic diagram of a pentacene dimer embedded within an optical cavity. An optical wavelength in the infrared regime, resonant with a specific coupling mode, was employed to facilitate effective light-matter interaction within the molecular system. Using a model Hamiltonian and specified parameters, we computed the PESs, as schematically depicted in Fig. 1(b).

Firstly, to investigate the nonadiabatic dynamics of the dimer, we initialized the system in the lowest vibrational level of excited state $|S_1\rangle$ indicated by the "X" mark in Fig. 1(b), representing the post-photoexcitation state. A CI between the PESs of states $|e_1\rangle$ and $|e_2\rangle$ (two electronic excited states in the adiabatic basis) was identified and plays a critical role in the subsequent dynamics. The evolution of the wave packet was computed using a quantum master equation approach. From this, we obtained the time-resolved reduced density matrix and performed a projection analysis to elucidate the population dynamics across the PESs. A detailed comparison between the Bloch-type master equation and the Redfield formalism is provided in the SI. In particular, Sections III–IV and Figs. S1-S3 demonstrate that the Bloch approach reliably reproduces population, coherence and wave-packet dynamics, thereby justifying its use for the present high-dimensional simulations.

As a preliminary step, we considered the dynamics in the absence of cavity interaction (i.e., $\eta = 0$). The time-

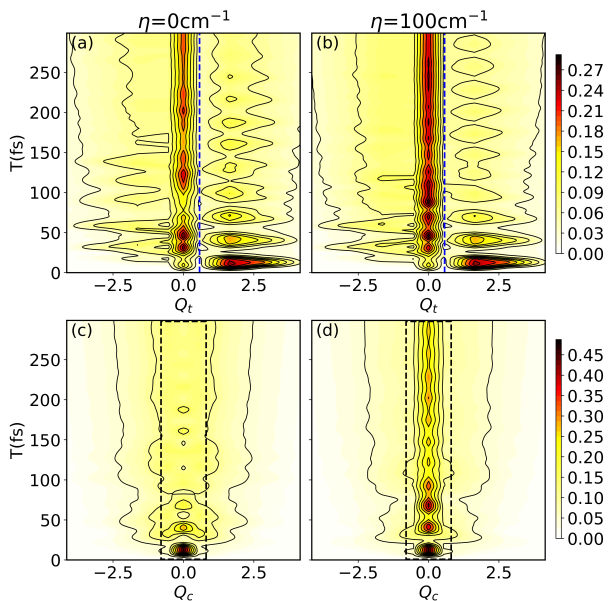


FIG. 2. (a, b) nuclear reduced density matrix associated with state $|e_1\rangle$ (lower electronic excited state in adiabatic basis) at $\eta = 0 \text{ cm}^{-1}$ and $\eta = 100 \text{ cm}^{-1}$, respectively. The blue dashed lines indicate the position of degenerate point between two PESs. (c, d) Corresponding nuclear reduced density matrix along the coupling coordinate Q_c (lower excited state). The black dashed boxes manifest the wave-packet cancellation along the center coordinate of Q_c .

resolved evolution of the wave packet is presented in Fig. 2. The associated projections along the Q_t and Q_c nuclear coordinates are shown in Fig. 2(a) and 2(c), respectively. Initially localized at the “X” point in Fig. 1(b), the wave packet evolves toward the CI, traverses it, and subsequently reaches the “Y” point. It then bifurcates along two distinct pathways en route to the minimum energy configuration denoted as “Z”. Owing to the GP accumulated during this evolution, destructive interference reduces the wave packet amplitude at the “Z” point. This effect is particularly evident in the Q_c -coordinate projection, as shown in Fig. 2(c), where the magnitude cancellation at Q_c substantiates this interference phenomenon.

B. Wave-packet dynamics of the dimer into a cavity

We investigated the influence of the optical cavity by systematically increasing the light-matter interaction strength, denoted by η , from 0 to 100 cm^{-1} . The resulting wave packet dynamics for $\eta = 100 \text{ cm}^{-1}$, analyzed via projection procedures, are presented in Fig. 2(b) and (d) (the results for $\eta = 30 \text{ cm}^{-1}$ are provided in the SI). These results reveal distinct modifications in the wave packet evolution along both the Q_t and Q_c nuclear coordinates. Notably, Fig. 2(d) highlights a significant en-

hancement in the central amplitude along Q_c compared to the $\eta = 0 \text{ cm}^{-1}$ case shown in Fig. 2(c). This enhancement indicates a disruption of the phase cancellation previously induced by the GP, suggesting that interaction with the cavity-coupled vibrational mode perturbs the stability of the GP interference. Comparison of the data for $\eta = 30 \text{ cm}^{-1}$ further confirms the trend that stronger coupling to the optical cavity progressively diminishes the influence of the GP on the wave packet interference. Overall, these findings illustrate that the destructive interference of the wave packet amplitude at the “Z” point in Fig. 1(b), a hallmark of GP effects, can be effectively modulated through coupling the CI system to an optical cavity resonant with the vibrational coupling mode.

To examine the interplay between the optical cavity and GP effects in the CI system, we analysed population dynamics under cavity coupling at visible wavelengths and with the cavity resonant to the tuning mode. Projection-based results, detailed in the SI, show that coupling to the tuning mode (optical or infrared) produces no significant modification of the GP dynamics. Accordingly, we focus subsequent analysis on cavity coupling to the coupling mode, using 2DES to further elucidate the resulting GP phenomena.

C. Two-dimensional Spectroscopy

To facilitate the optical detection of GP effects, we performed 2DES simulations at waiting time of 50 fs. The computed spectra are presented in Fig. 3. The theoretical framework and computational details for the response function and 2DES simulations are outlined in the SI. For these spectroscopic calculations, we initialized the wave packet in the lowest vibrational level of the electronic ground state, providing a well-defined starting point for the subsequent dynamical evolution, which gives us $\rho(0) = |S_0, n_c = 0, n_t = 0, n_a = 0\rangle\langle n_a = 0, n_t = 0, n_c = 0, S_0|$. Fig. 3(a) presents the 2DES at a waiting time of $T = 50 \text{ fs}$ in the absence of cavity coupling, while Fig. 3(b) shows the corresponding spectrum for $\eta = 100 \text{ cm}^{-1}$. A pronounced difference is observed at $\omega_t = 10.6 \text{ kcm}^{-1}$, where additional main and cross peaks emerge upon coupling to the cavity. To substantiate the assignment of these features, we diagonalized the vibronic Hamiltonian for both $\eta = 0 \text{ cm}^{-1}$ and $\eta = 100 \text{ cm}^{-1}$. This analysis confirms that the dominant diagonal signals arise from ground-state bleach pathways, whereas the prominent blue cross-peak (peak B) originates from an ESA transition from the Z-region of the lower adiabatic surface to the second excited manifold. The amplitude of this ESA feature directly reflects the nuclear wave-packet distribution at the CI geometry. In the absence of cavity coupling ($\eta = 0 \text{ cm}^{-1}$), GP-induced destructive interference cancels the wave-packet amplitude at this point, thereby suppressing the ESA peak. Introducing cavity coupling perturbs the nuclear symmetry, reduces this interference, and restores the ESA in-

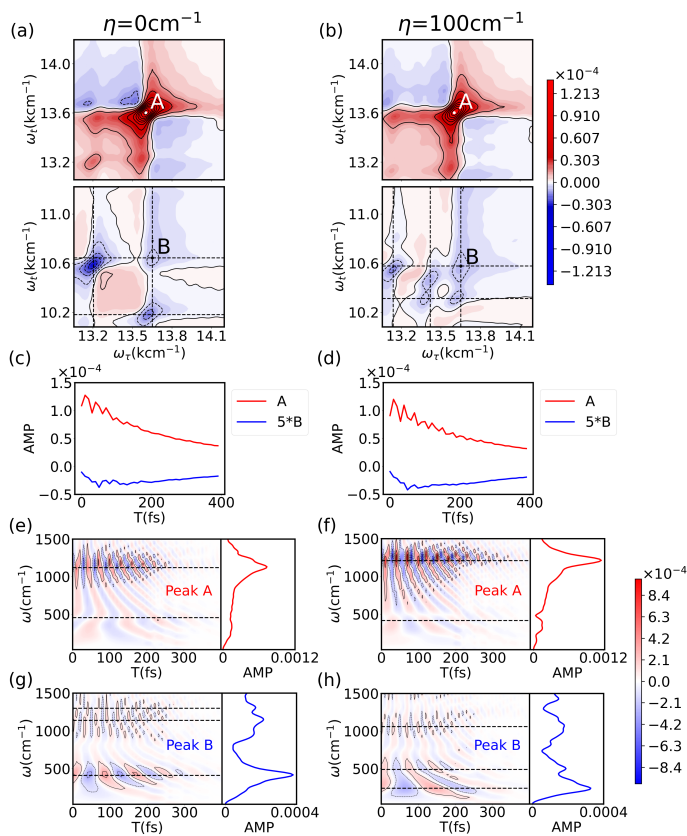


FIG. 3. Two-dimensional electronic spectroscopy and wavelet analyses for varying η . Panels (a, b) show 2DES maps at $T = 50$ fs for $\eta = 0$ and 100 cm^{-1} , revealing ESA-induced spectral changes. Panels (c, d) depict time-domain traces of Peaks A and B. Panels (e-h) show wavelet-transformed coherence maps, highlighting frequency- and time-resolved modulations due to GP effects under vibronic-cavity coupling.

tensity. This behavior is reproduced across intermediate values of η , demonstrating the progressive recovery of the ESA peak with increasing coupling strength (Fig. S9). Full transition assignments and the associated eigenvalue analysis are provided in Section VII of the SI (Fig. S4), confirming that the ESA transition identified in Fig. 1(b) serves as a direct spectroscopic signature of GP-induced interference.

To gain deeper insights into population dynamics and coherent behavior, we extended the 2DES simulations by increasing the number of time steps. Two distinct spectral features, labeled as peaks A and B, were selected for detailed analysis. The corresponding time-resolved signals are presented in Fig. 3(c) and (d), with the temporal traces shown as red and blue solid lines in Fig. 3(c) for the case where the coupling strength $\eta = 0$ cm^{-1} . Following the subtraction of kinetic components through exponential fitting, a Fourier transform was applied to the residuals to extract oscillatory components. The resulting frequency spectra revealed prominent oscillations at 250 and 1200 cm^{-1} for both peaks. Subsequently, we

investigated the effect of nonzero coupling by simulating 2DES for $\eta = 100$ cm^{-1} . The temporal evolution of peaks A and B for $\eta = 30$ cm^{-1} is displayed in SI along with its Fourier-transformed spectra. Peak A (red trace) continued to exhibit oscillatory frequencies at 250 and 1200 cm^{-1} . However, peak B (blue trace) displayed a distinct spectral shift, with oscillations at 300 and 1350 cm^{-1} , indicating a blue shift relative to the $\eta = 0$ cm^{-1} case. For $\eta = 100$ cm^{-1} , with corresponding time-domain traces illustrated in Fig. 3(d) and their frequency-domain representations in Fig. 3(f) along the Y-axis. Here, the red trace (peak A) retained the 1200 cm^{-1} mode, while the low-frequency component disappeared. Conversely, the blue trace (peak B) exhibited an amplified low-frequency component and a red-shifted peak around 1000 cm^{-1} . These findings demonstrate that 2DES can resolve and isolate spectral signatures linked to the GP near a CI, as modulated by varying the coupling strength between the cavity and vibrational modes. To explore this behavior systematically, additional wave-packet dynamics and 2DES simulations were conducted with η incremented in steps of 10 cm^{-1} . Comprehensive results from this parameter sweep are provided in the SI.

To further investigate the time-resolved coherence, we conducted a wavelet analysis on the residual signals and present the corresponding results in Fig. 3(e)-(h). Fig. 3(e) illustrates the temporal evolution of coherence at frequencies of 1200 cm^{-1} and 250 cm^{-1} . The high-frequency component at 1200 cm^{-1} exhibits pronounced oscillations that vanish around 100 fs, while the low-frequency mode decays within 200 fs. Notably, the coherence characteristics of peak B, as shown in Fig. 3(g), exhibit behavior remarkably similar to those of peak A. Further analysis for $\eta = 100$ cm^{-1} is presented in Fig. 3(f) and (h), corresponding to peaks A and B, respectively. Both figures reveal the presence of high- and low-frequency modes. Interestingly, in Fig. 3(f), the amplitude of the low-frequency mode is diminished, while the high-frequency coherence is enhanced. In contrast, Fig. 3(h) shows a markedly different trend: the high-frequency mode exhibits significantly reduced amplitude and shortened lifetime, whereas the low-frequency mode becomes more prominent. These observations underscore the sensitivity of coherence dynamics to the coupling strength parameter η and highlight how wavelet analysis complements Fourier-based approaches by providing temporal resolution of frequency-dependent coherence lifetimes.

To elucidate the influence of cavity-molecule coupling on coherent dynamics, we calculated the 2DES by varying the η from 0 to 100 cm^{-1} in increments of 10 cm^{-1} . This allowed us to systematically track the evolution of coherence lifetimes for selected spectral features, denoted as Peaks A and B. Time-domain signals were extracted and fit with exponential decay functions to determine coherence lifetimes, as summarized in Fig. 4. Fig. 4(a) reveals that the lifetime of Peak A, associated with GSB, exhibits a pronounced increase near η

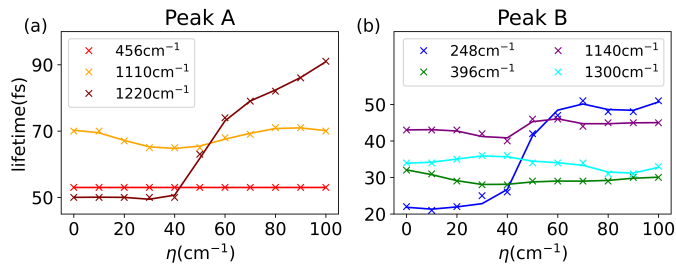


FIG. 4. Extracted coherence lifetimes of vibrational modes for Peaks A (a) and B (b) as a function of cavity-molecule coupling strength η . Peak A reflects GSB dynamics, while Peak B captures ESA behavior. Enhanced lifetimes, especially for low-frequency modes, indicate GP effects near a CI under strong coupling.

$= 50 \text{ cm}^{-1}$, highlighting the sensitivity of GSB signals to vibrational strong coupling. In contrast, Fig. 4(b) presents the lifetime trends for Peak B, which originates from ESA. Here, a distinct change in coherence lifetime is also observed around $\eta = 50 \text{ cm}^{-1}$, most notably for the 248 cm^{-1} mode, whose lifetime significantly increases with stronger coupling. These results underscore the role of cavity-enhanced vibronic interactions in modulating wave packet dynamics. In particular, the extended coherence lifetime of the low-frequency ESA mode (248 cm^{-1}) provides direct evidence of reduced wave packet cancellation, consistent with the influence of GP near a CI. Full computational details and additional analyses are provided in the Supporting Information. Overall, these findings establish 2DES as a powerful tool for detecting GP-induced interference effects in strongly coupled light-matter systems.

DISCUSSIONS

Cavity-modulated dynamics at CI offer a compelling approach for studying quantum coherent control in molecular systems. By combining 2DES with optical cavities, our work provides new understanding of topological effects in molecular wave packet evolution, especially the GP tied to CIs. We show that cavity-induced modulation can isolate spectroscopic signatures of the GP by selectively influencing wave packet pathways. Conventional transient absorption spectroscopy alone cannot resolve the GP signature identified here. The coherent oscillations linked to cross-peak B spectrally overlap with dominant diagonal features along the excitation axis, rendering them indistinguishable in one-dimensional measurements. In contrast, 2DES disentangles excitation and detection frequencies, isolating this cross-peak and clearly revealing its oscillatory component. Such frequency-resolved separation is thus crucial for exposing the interference arising from the GP.

The cavity's spectral tunability, from visible to tera-

hertz, enables precise manipulation of quantum dynamics. When coupled with the temporal resolution of 2DES, this setup allows detailed tracking of excited-state evolution. The strong nonadiabatic coupling near CI amplifies these quantum features, enhancing sensitivity to external perturbations. This creates opportunities not just for probing but actively steering molecular reactions. Such control is particularly valuable for processes like photoisomerization and singlet fission, which are central to biological vision, solar energy harvesting, and molecular optoelectronics. In realistic molecular systems such as crystalline pentacene, numerous vibrational modes couple to electronic states, disrupting the ideal symmetry of the potential-energy surfaces and obscuring GP interference. Hence, selecting molecules with simpler excited-state topology and well-defined tuning and coupling coordinates is essential. Although pyrazine is a promising candidate, its ultraviolet absorption and weak transition dipole impose practical constraints for current 2DES experiments.

Beyond molecular systems, this approach has strong parallels to emerging themes in quantum materials and topological photonics[41–43]. Recent studies have shown that optical cavities can influence phase transitions, electronic structures, and correlated electron dynamics in solid-state systems[44, 45]. Similarly, structured light and spatial light modulators are increasingly employed to control exotic states of matter, such as polariton condensates and Floquet topological insulators[46]. Our work situates itself at the intersection of these fields, suggesting that cavity-modulated molecular systems can serve as analog platforms for studying broader quantum phenomena under controlled conditions.

Looking forward, this research opens several compelling avenues. Experimentally, realizing cavity-modulated spectroscopy in the ultrafast regime will require precise cavity designs and tailored light-matter interaction schemes, but the technological progress in nanophotonics and cavity-QED makes this feasible. Theoretically, the inclusion of more complex vibrational modes, solvent environments, and entangled electronic states could further enrich the model and bring it closer to real molecular systems. Future efforts could also explore quantum entanglement generation, non-Hermitian dynamics near CIs, and quantum thermodynamic implications of topological phases in molecular reactions. In summary, our study provides a fundamental step toward unifying concepts of GP, nonadiabatic dynamics, and quantum control through the lens of cavity-modulated spectroscopy. This approach offers a versatile and deeply insightful platform for advancing both molecular physics and the broader field of quantum science.

CONCLUSIONS

In this study, we investigated the wave-packet dynamics influenced by the GP in the vicinity of a CI. We be-

gan by analyzing the population dynamics and examining the differences in wave-packet behavior under varying strengths of cavity-molecule coupling. This systematic approach enabled us to refine the relevant parameters and identify an optimal model capable of capturing distinct signatures of the GP. With these optimized parameters and an appropriately constructed Hamiltonian, we computed the corresponding 2DES. The resulting spectra revealed clear and robust evidence of the GP, thereby demonstrating that the proposed molecular system, under cavity modulation, serves as a reliable platform for detecting such topological effects. Our findings establish a compelling framework for exploring the GP within CI-mediated nonadiabatic dynamics using spectroscopic methods. Notably, this work offers not only a theoretical protocol but also a potential experimental design for directly identifying the GP, and by extension, confirming the existence of a CI in molecular systems. This approach paves the way for further advancements in quantum con-

trol, coherent light-matter interactions, and the fundamental understanding of topological effects in molecular and condensed-phase systems.

Acknowledgements This work was supported by National Key Research and Development Program of China (Grant No. 2024YFA1409800), NSFC Grant with No. 12274247, Yongjiang talents program with No. 2022A-094-G and 2023A-158-G, Ningbo International Science and Technology Cooperation with No. 2023H009, ‘Lixue+’ Innovation Leading Project and the foundation of national excellent young scientist. The Next Generation Chemistry theme at the Rosalind Franklin Institute is supported by the EPSRC (V011359/1 (P)) (AJ).

Author contributions: H.-G. D. conceived the research project. Y.C.Y. performed the calculations. H.-G.D. F. Z. and A.J. wrote the first draft of manuscript. All authors contributed towards the refinement of the manuscript. H.-G. D. supervised this project.

-
- [1] W. Domcke, D. R. Yarkony, H. Köppel, *Conical Intersections: Theory, Computation and Experiment*; World Scientific: Singapore, 2011.
- [2] W. Domcke, D. R. Yarkony, *Role of Conical Intersections in Molecular Spectroscopy and Photo-induced Chemical Dynamics*. *Annu. Rev. Phys. Chem.* **63**, 325 (2012).
- [3] M. Kowalewski, B. P Fingerhut, K. E Dorfman, K. Bennett, S. Mukamel, *Simulating Coherent Multidimensional Spectroscopy of Nonadiabatic Molecular Processes: From the Infrared to the X-ray Regime*. *Chem. Rev.* **117**, 12165 (2017).
- [4] M. Born and R. Oppenheimer. *Zur Quantentheorie der Molekeln*. In: *Annalen der Physik* 389.20 pp. 457-484, (1927).
- [5] Y. Chang, T. Balciunas, Z. Yin, M. Sapunar, B. N. C. Tenorio, A. C. Paul, and S. Tsuru. *Electronic dynamics created at conical intersections and its dephasing in aqueous solution*. *Nature Physics* **21**, 137-145 (2025).
- [6] Y. Boeije, and M. Olivucci. *From a one-mode to a multi-mode understanding of conical intersection mediated ultrafast organic photochemical reactions*. *Chem. Soc. Rev.* **52**, 2643-2687 (2023).
- [7] M. Barbatti, A. J. A. Aquino, J. J. Szymczak, D. Nachtigallová, P. Hobza, and H. Lischka. *Relaxation mechanisms of UV-photoexcited DNA and RNA nucleobases*. *Proc. Natl. Acad. Sci. (USA)* **107**, 21453-21458 (2010).
- [8] A. Jha, *et al.*, *Origin of poor doping efficiency in solution processed organic semiconductors*. *Chemical Science* **9**, 4468-4476 (2018).
- [9] A. J. Musser, M. Liebel, C. Schnedermann, T. Wende, T. B. Kehoe, A. Rao & P. Kukura, *Evidence for conical intersection dynamics mediating ultrafast singlet exciton fission*. *Nature Phys.* **11**, 352 (2015).
- [10] H.-G. Duan *et al.* *Intermolecular vibrations mediate ultrafast singlet fission*. *Science Adv.* **6**, abb0052 (2020).
- [11] P. Kukura, D. W. McCamant, S. Yoon, D. B. Wand-schneider, and R. A. Mathies, *Structural Observation of the Primary Isomerization in Vision with Femtosecond-Stimulated Raman*. *Science* **310**, 1006 (2005).
- [12] S. Takeuchi, S. Ruhman, T. Tsuneda, M. Chiba, T. Taketsugu, and T. Tahara, *Spectroscopic Tracking of Structural Evolution in Ultrafast Stilbene Photoisomerization*. *Science* **322**, 1073 (2008).
- [13] P. J. M. Johnson, A. Halpin, T. Morizumi, V. I. Prokhorenko, O. P. Ernst & R. J. D. Miller, *Local vibrational coherences drive the primary photochemistry of vision*. *Nature Chem.* **7**, 980 (2015).
- [14] P. J. M. Johnson, M. H. Farag, A. Halpin, T. Morizumi, V. I. Prokhorenko, J. Knoester, T. L. C. Jansen, O. P. Ernst, R. J. D. Miller. *The Primary Photochemistry of Vision Occurs at the Molecular Speed Limit*. *J. Phys. Chem. B* **121**, 4040 (2017).
- [15] C. Schnedermann, A. M. Alvertis, T. Wende, S. Lukman, J. Feng, F. A. Y. N. Schröder, D. H. P. Turban, J. Wu, N. D. M. Hine, N. C. Greenham, A. W. Chin, A. Rao, P. Kukura & A. J. Musser. *A molecular movie of ultrafast singlet fission*. *Nature Comm.* **10**, 4207 (2019).
- [16] K. Miyata, Y. Kurashige, K. Watanabe, T. Sugimoto, S. Takahashi, S. Tanaka, J. Takeya, T. Yanai & Y. Matsumoto, *Coherent singlet fission activated by symmetry breaking*. *Nature Chem.* **9**, 983 (2017).
- [17] B. Gu. *et al.* *Optical-Cavity Manipulation of Conical Intersections and Singlet Fission in Pentacene Dimers*. *J. Phys. Chem. Lett.* **12**, 2052 (2021).
- [18] M. H. Farag, *et al.* *Polariton Induced Conical Intersection and Berry Phase*. *Phys. Chem. Chem. Phys.* **23**, 16868 (2021).
- [19] C. Fábri, *et al.* *Classical and quantum light-induced non-adiabaticity in molecular systems*. *AVS Quant. Sci.* **6**, 023501 (2024).
- [20] L. A. Martínez-Martínez, *et al.* *Polariton-Assisted Singlet Fission in Acene Aggregates*. *J. Phys. Chem. Lett.* **15**, 4655 (2024).
- [21] L. Chen, M. F. Gelin, V. Y. Chernyak, W. Domcke and Y. Zhao, *Dissipative dynamics at conical intersections: simulations with the hierarchy equations of motion method*. *Faraday Discussions*, **194**, 61 (2006).
- [22] S. Krempl, W. Domcke, M. Winterstetter, *Real-time*

- path-integral approach for general two-state multi-mode vibronic-coupling models. *Chem. Phys.* **206**, 63 (1996).
- [23] R. González-Luque, M. Garavelli, F. Bernardi, and M. Olivucci, Computational evidence in favor of a two-state, two-mode model of the retinal chromophore photoisomerization. *Proc. Natl. Acad. Sci. (USA)* **97**, 9379 (2000).
- [24] L. Chen, M. F. Gelin, Y. Zhao, W. Domcke, Mapping of Wave Packet Dynamics at Conical Intersections by Time- and Frequency-Resolved Fluorescence Spectroscopy: A Computational Study. *J. Phys. Chem. Lett.* **10**, 5873 (2019).
- [25] E. Mangaud, *et al.* Statistical distributions of the tuning and coupling collective modes at a conical intersection using the hierarchical equations of motion. *J. Chem. Phys.* **151**, 244102 (2019).
- [26] A. J. Schile D. T. Limmer, Simulating conical intersection dynamics in the condensed phase with hybrid quantum master equations. *J. Chem. Phys.* **151**, 014106 (2019).
- [27] J. Krčmář, M. F. Gelin, D. Egorova and W. Domcke, Signatures of conical intersections in two-dimensional electronic spectra. *J. Phys. B* **47**, 124019 (2014).
- [28] H. -G. Duan *et al.* Quantum Mechanical Wave Packet Dynamics at a Conical Intersection with Strong Vibrational Dissipation. *J. Phys. Chem. Lett.* **7**, 382 (2016).
- [29] H. -G. Duan *et al.* Impact of Vibrational Coherence on the Quantum Yield at a Conical Intersection. *J. Phys. Chem. Lett.* **7**, 3491 (2016).
- [30] M. Sala, D. Egorova. Two-dimensional photon-echo spectroscopy at a conical intersection: A two-mode pyrazine model with dissipation. *Chem. Phys.* **481**, 206 (2016).
- [31] D. Keefer, T. Schnappinger, R. de Vivie-Riedle, and S. Mukamel, Visualizing conical intersection passages via vibronic coherence maps generated by stimulated ultrafast X-ray Raman signals. *Proc. Natl. Acad. Sci. (USA)* **117**, 24069 (2020).
- [32] D. Cho and S. Mukamel, Stimulated X-ray Raman Imaging of Conical Intersections. *J. Phys. Chem. Lett.* **11**, 33 (2020).
- [33] H. Yong, *et al.* Direct Monitoring of Conical Intersection Passage via Electronic Coherences in Twisted X-Ray Diffraction. *Phys. Rev. Lett.* **129**, 103001 (2022).
- [34] D. Jadoun, M. Kowalewski, Time-Resolved Photoelectron Spectroscopy of Conical Intersections with Attosecond Pulse Trains. *J. Phys. Chem. Lett.* **12**, 8103 (2021).
- [35] M. Kowalewski, *et al.* Catching Conical Intersections in the Act: Monitoring Transient Electronic Coherences by Attosecond Stimulated X-Ray Raman Signals. *Phys. Rev. Lett.* **115**, 193003 (2015).
- [36] H. -G. Duan, D. -L. Qi, Z. -R. Sun, R. J. D. Miller, M. Thorwart. Signature of the geometric phase in the wave packet dynamics on hypersurfaces. *Chem. Phys.* **515**, 21 (2018).
- [37] K. Sun, *et al.* Optical-cavity manipulation strategies of singlet fission systems mediated by conical intersections: Insights from fully quantum simulations. *J. Chem. Phys.* **162**, 130902 (2025).
- [38] Martínez-Martínez, L. A. *et al.* Polariton-Assisted Singlet Fission in Acene Aggregates. *J. Phys. Chem. Lett.* **9**, 1951 (2018).
- [39] D. Qi, *et al.* Tracking an electronic wave packet in the vicinity of a conical intersection. *J. Chem. Phys.* **147**, 074101 (2017).
- [40] L. Chen, M. F. Gelin, W. Domcke, Multimode quantum dynamics with multiple Davydov D2 trial states: Application to a 24-dimensional conical intersection model. *J. Chem. Phys.* **150**, 024101 (2019).
- [41] C. Schäfer, M. Ruggenthaler, H. Appel, and A. Rubio. Modification of excitation and charge transfer in cavity quantum-electrodynamical chemistry. *Proc. Natl. Acad. Sci. (USA)* **116**, 4883 (2019).
- [42] F. Schlawin, D. M. Kennes, and M. A. Sentef. Cavity quantum materials. *App. Phys. Rev.* **9**, 011314 (2022).
- [43] J. Bloch, A. Cavalleri, V. Galitski, M. Hafezi & A. Rubio, Strongly correlated electron-photon systems. *Nature* **606**, 41-48 (2022).
- [44] H. Hübener, U. De Giovannini, C. Schäfer, J. Andberger, M. Ruggenthaler, J. Faist & A. Rubio, Engineering quantum materials with chiral optical cavities. *Nature Mater.* **20**, 438 (2020).
- [45] J. A. Muniz, D. Barberena, R. J. Lewis-Swan, D. J. Young, J. R. K. Cline, A. Maria Rey & J. K. Thompson, Exploring dynamical phase transitions with cold atoms in an optical cavity. *Nature* **580**, 602-607 (2020).
- [46] S. Mukherjee & M. C. Rechtsman, Observation of Floquet solitons in a topological band gap. *Science* **368**, 856-859 (2020).
- [47] S. Mukamel. Principles of nonlinear optical spectroscopy, Oxford University Press, New York. (1995).